Supporting Information

Zhou et al. 10.1073/pnas.1705509114

SI Text

Fabrication of Syringe-Injectable Mesh Electronics. The syringe-injectable mesh electronics used in these studies had design parameters similar to previous reports (23, 25, 26) with (*i*) total mesh width, $W = 2$ mm; (*ii*) widths of longitudinal SU-8 elements, $w_1 = 20$ μm, and transverse SU-8 elements, $w_2 = 20$ μm; (*iii*) angle between longitudinal and transverse elements, $\alpha = 45°$; (*iv*) spacing or pitch of the transverse elements, $L_1 = 333$ μm, and longitudinal elements, $L_2 = 250$ μm; (*v*) gold interconnect line width, $w_m = 10$ μm; and (*vi*) three-layer sandwich structure (SU-8 polymer/metal/SU-8 polymer, as indicated in Fig. 1*A*, *II*) for longitudinal ribbons and two-layer structure (SU-8 polymer/SU-8 polymer) for transverse ribbons. The mesh electronics fabrication was carried out using published methods (26, 28) with key steps as follows. (*i*) A 100-nm-thick sacrificial layer of Ni was thermally evaporated onto a 3-inch Si wafer (600-nm thermal oxide; Nova Electronic Materials), which was precleaned in an oxygen plasma (50 W, 1 min). (*ii*) Negative photoresist SU-8 (SU-8 2000.5; MicroChem Corp.) was spin-coated on the wafer to a thickness of *ca*. 420 nm, prebaked sequentially at 65 °C for 1 min and 95 °C for 4 min, and then patterned to the bottom layer mesh structure by PL. After PL exposure the sample was postbaked sequentially at 65 °C for 1 min and 95 °C for 3 min. (*iii*) The SU-8 photoresist was then developed (SU-8 Developer; MicroChem Corp.) for 1.5 min, rinsed with isopropanol, dried in a N_2 flow, and hard-baked at 180 °C for 1 h. (*iv*) The wafer was then cleaned in an oxygen plasma (50 W, 1 min), spin-coated with MCC Primer 80/20 and LOR 3A lift-off resist (MicroChem Corp.), and baked at 180 °C for 5 min. After cooling, the wafer was spin-coated with Shipley 1805 positive photoresist (Microposit; Dow Chemical Company), baked at 115 °C for 4 min, and then the pattern for metal features was defined by PL and developed in MF-CD-26 (Microposit; Dow Chemical Company) for 90 s. (*v*) A 5-nm-thick Cr layer and a 100-nm-thick Au layer were thermally evaporated, followed by a lift-off step (Remover PG; MicroChem Corp.) (*vi*) Steps *iv* and *v* were repeated for patterning and deposition of the Pt sensing electrodes (Cr/Pt, 5 nm/50 nm). (*vii*) Steps *ii* and *iii* were repeated for patterning the top SU-8 layer, which was aligned to the bottom SU-8 layer and served to fully encapsulate the metal interconnect lines but not the Pt sensing electrodes. (*viii*) Finally, the Si wafer was cleaned in an oxygen plasma (50 W, 1 min), and then transferred to a Ni etchant solution (40% $FeCl_3$:39% HCl:H_2O = 1:1:20) to remove the sacrificial Ni layer and release the mesh electronics from the Si substrate.

Effective Bending Stiffness of Implanted Probes. The effective bending stiffness per width of the three-layer longitudinal ribbon elements in the mesh, D_1, can be estimated as (45)

$$D_1 = \frac{1}{w_1}\left(\frac{E_s(h-h_m)^3 w_1}{12} + \frac{E_m h_m^3 w_m}{12}\right), \qquad \textbf{[S1]}$$

where E_s is Young's modulus of SU-8, E_m is Young's modulus of gold, h is the total ribbon thickness, h_m is the metal thickness, w_1 is the width of the SU-8 ribbon elements, and w_m is the width of metal. The Young's modulus values are $E_s = 2$ GPa and $E_m = 79$ GPa (26), and with other experimental values of $h = 948 \pm 10$ (SD) nm, $h_m = 105$ nm, $w_1 = 20$ μm, and $w_m = 10$ μm, then yields $D_1 = 0.104 \pm 0.005$ (SD) nN·m.

The effective bending stiffness of the longitudinal ribbon elements of the mesh was also estimated with finite element software ABAQUS as reported previously (23). The composite cross-section of the longitudinal ribbon consists of two layers of SU-8 with total thickness of 843 nm, width of 20 μm and a 105-nm-thick gold layer with width of 10 μm between the two SU-8 layers (as indicated by the cross-section view in Fig. 1*A*, *II*). Young's moduli of 2 GPa for SU-8 and 79 GPa for gold (as above) were used in the simulation with the longitudinal ribbon treated as a free beam. The simulated bending stiffness of a single longitudinal ribbon, 0.125 nN·m, is consistent with the value determined above using Eq. **S1**, and the longitudinal and transverse bending stiffness values determined from our previous simulation of the mesh 2D single unit cell (23).

The effective bending stiffness per width of standard polyimide flexible thin-film probes (30), D_2, is given by (45)

$$D_2 = E_p \frac{h_p^3}{12}, \qquad \textbf{[S2]}$$

where E_p is the Young's modulus of polyimide and h_p is the thickness of the probe. When $E_p = 2.5$ GPa and $h_p = 25$ μm, then $D_2 = 3.3 \times 10^3$ nN·m.

Vertebrate Animal Subjects. Adult male C57BL/6J mice (Jackson Laboratory) were used in this study. All procedures performed on the mice were approved by the Animal Care and Use Committee of Harvard University. The animal care and use programs at Harvard University meet the requirements of the federal law (89-544 and 91-579) and NIH regulations and are also accredited by the American Association for Accreditation of Laboratory Animal Care. Animals were group-housed on a 12-h:12-h light:dark cycle in Harvard University's Biology Research Infrastructure and given food and water for ad libitum consumption as appropriate.

Stereotaxic Surgery and Probe Implantation. Key steps for in vivo implantation of mesh or polyimide flexible thin-film electronic probes into live mice brains include the following. (*i*) All probes were sterilized with 70% ethanol before use. Mesh electronics were sterilized with 70% ethanol and rinsed in sterile deionized water then transferred into sterile 1× PBS. Flexible thin-film probes (25 μm in thickness, *ca*. 500 μm in width) were sterilized with 70% ethanol and dried with nitrogen. (*ii*) Mice were anesthetized through i.p. injection of a mixture of ketamine (75 mg/kg; Patterson Veterinary Supply Inc.) and dexdomitor (1 mg/kg; Orion Corp.) and verified via toe pinch before surgery. A heating pad (37 °C) was placed under mice during surgery to maintain appropriate body temperature. (*iii*) Mouse hair was removed using lotion (Nair; Church & Dwight) and iodophor was applied to sterilize the depilated scalp skin. (*iv*) A 1-cm longitudinal incision along the sagittal sinus was made and the skin was resected to expose a 5- × 5-mm portion of the skull. (*v*) A 1-mm-diameter hole was drilled using a dental drill (micromotor with on/off pedal 110/220; Grobet USA) with stereotaxic coordinates of anteroposterior −1.70 mm and mediolateral 2.00 mm, and the dura was removed. (*vi*) Flexible thin-film probes were inserted 4 mm into the mouse brain through the hole; mesh electronics were loaded into a glass capillary needle with i.d. of 400 μm and o.d. of 650 μm (Produstrial LLC) and then injected into the mouse brain using our reported controlled injection procedure (25). The wound is sealed by applying Metabond enamel etchant gel (Parkell Inc.) over the exposed cranial bone

and the skin was sealed by using 3M Vetbond Tissue Adhesive (Santa Cruz Biotechnology Inc.)

Postoperative Care of Animals. Antibiotic ointment (WATER-JEL Technologies) was applied copiously around the wound after surgery. The mouse was returned to a cage equipped with a 37 °C heating pad and its activity monitored every hour until it fully recovered from anesthesia. Buprenex (buprenorphine; Patterson Veterinary Supply Inc.) was administered intraperitoneally at a dose of 0.05 mg/kg body weight every 12 h for up to 72 h postsurgery.

Histology Sample Preparation for Horizontal Sections. Mice implanted with mesh or flexible thin-film probes at postinjection/implantation times of 2 wk, 4 wk, and 3 mo were anesthetized with ketamine and dexdomitor as above and then were transcardially perfused with 1× PBS, followed with 4% formaldehyde (Sigma-Aldrich) before decapitation. The scalp skin was removed and exposed skull at the probe insertion site was ground for 10–20 min at 10,000 rpm using a high-speed rotary tool (Dremel). The brain was resected from the cranium and placed in 4% formaldehyde for 24 h to fix brain tissue and then transferred to 1× PBS for another 24 h at 4 °C to remove remaining formaldehyde. The brain was transferred to incrementally increasing sucrose solutions (10–30%) (Sigma-Aldrich) at 4 °C to cryoprotect the tissue. Then, the brain was transferred to optimum cutting temperature compound (Tissue-Tek O.C.T. Compound; VWR) and frozen at −80 °C. The frozen sample was sectioned into 10-μm-thick horizontal slices using a Leica CM1950 cryosectioning instrument (Leica Microsystems).

Histology Sample Preparation for Sagittal Sections. Mice implanted with mesh electronics probes at 3 mo postimplantation were transcardially perfused, and then the brains were resected as described above in the preparation of horizontal sections. The brains were placed in 4% formaldehyde for 24 h and then transferred to 1× PBS for another 24 h at 4 °C to remove remaining formaldehyde. The brains were then embedded in 3% agarose (SeaPlaque Lonza Group Ltd.) hydrogel, cut into cubes of 1 cm (height) × 2 cm (length) × 2.5 cm (width), and imaged by micro-CT to define the polar angle θ in the spherical coordinate system (usually less than 15°) between the surface of the hydrogel and the longitudinal axis of the mesh probe. The hydrogel cubes were then cut using a homemade sectioning machine according to measured angle θ to make one surface of the cube parallel to the longitudinal axis of the implanted mesh and also parallel to the midline of the brain. The cubes with this defined surface/probe orientation were then mounted on a vibratome (VT1000 S vibrating blade microtome; Leica) stage and sectioned into 200-μm slices.

Imaging and Image Data Analysis. Confocal fluorescence microscopy images were acquired on a Zeiss LSM 880 confocal microscope (Carl Zeiss Microscopy GmbH). Confocal images of antibody-labeled horizontal slices in Fig. 2 and Fig. S2 were acquired using 488-, 561-, and 633-nm lasers as the excitation sources for Alexa Fluor 488, Alexa Fluor 568, and Alexa Fluor 647, respectively, and a 1-AU pinhole. The mesh electronics in each slice was imaged with DIC on the same microscope (Fig. S1). Mesh electronics elements were extracted from DIC images as false blue color using MATLAB. The extracted images were then merged with corresponding confocal images using ImageJ software for composite images shown in Fig. 2 and Fig. S2. Images of flexible thin-film probes were acquired using the same method, where the flexible thin-film probes are assigned a false blue color in the composite images. Confocal images of the antibody-labeled sagittal slice in Fig. 4 were acquired using the same excitation sources as above, a 3-AU pinhole, which yields an optical section thickness of *ca*. 9 μm, and imaging plane centered at *ca*. 5 μm below the surface of the sample. The mesh electronics in Fig. 4 were imaged with reflection mode of the same confocal microscope by collecting reflected photons with zero Stokes shift off the highly reflective metal interconnect lines in the mesh and the same 3-AU pinhole (Fig. S5). The mesh electronics elements were extracted from reflection images as a false blue color using MATLAB and then merged with corresponding confocal images using ImageJ software for composite images shown in Fig. 4. Both sides of the sagittal slice were imaged with the same method and shown in Fig. 4*A* (side-A) and Fig. 4*B* (side-B), respectively.

Custom MATLAB software was used for analysis of the fluorescence intensity in confocal microscope images. Fluorescence intensities of NF, NeuN, GFAP, and Iba-1 were analyzed based on zoomed-out images of those shown in Fig. 2 and Fig. S2 with a field of view of 1,275 μm × 1,275 μm and the images in Fig. 4. The analysis procedure was the similar for all of these images and follows the specific example of the horizontal-slice shown in Fig. S4, from a zoom-out of Fig. 2*B*, *IV*. First, the mesh boundary was defined by a polygon (red-orange, Fig. S4) that is drawn to encompass all mesh ribbons tangentially. This mesh boundary separates all pixels in a given image into "interior" pixels (used for plotting within the pink shaded regions of Fig. 3) and "exterior" pixels (used for plotting outside the pink shaded regions of Fig. 3). The distance of each pixel from mesh electronics was defined as its shortest distance to the boundary of mesh electronics (the red-orange polygon). Pixels in the image were grouped according to the distances from mesh electronics. As shown in Fig. S4, all pixels on each of the green polygons share the same distance from the mesh boundary. The fluorescence intensity of each pixel was obtained and the intensity values for all pixels with distances binned over an interval of 20 μm were averaged and then normalized by the baseline intensity defined as the average fluorescence intensity of all pixels 500–520 μm away from the mesh boundary. The same method was used for the fluorescence intensity analysis of images in Figs. 2 and 4 and Fig. S2, including the flexible thin-film probes. For Fig. 4, NF and GFAP fluorescence intensity was analyzed based on entire images, whereas the NeuN fluorescence intensity was analyzed based on the regions shown in yellow dashed boxes. These boxed regions were selected to have a relatively homogeneous neuron distribution. The pink shaded regions in Figs. 3 and 4 indicate the interior of mesh electronics, and the zero distance corresponds to the surfaces of the mesh electronics and flexible thin-film probes.

Micro-CT Imaging and Analysis. Images (Fig. S3) and the orientations of injected mesh electronics probes in fixed mouse brain tissue at different times postimplantation (acute–3 mo) were determined using an HMXST micro-CT X-ray scanning system with a standard horizontal imaging axis cabinet (HMXST225; Nikon Metrology). Typical imaging parameters were 65 kV and 130 μA (no filter). Shading correction and flux normalization were applied before scanning to adjust the X-ray detector. CT Pro-3D software (Nikon-Metris) was used to calibrate centers of rotation and to reconstruct the images. VGStudio MAX software (Volume Graphics GMbh) was used for 3D rendering and analysis of the reconstructed images.

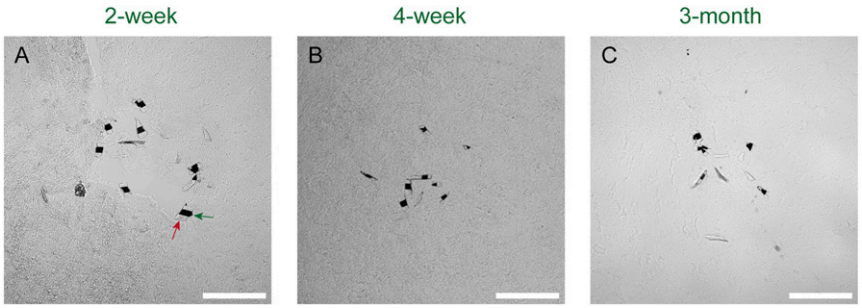

Fig. S1. DIC microscopy images of horizontal sectioned samples of implanted mesh electronics probes in mice brains at (*A*) 2 wk, (*B*) 4 wk, and (*C*) 3 mo postinjection. Longitudinal mesh elements with encapsulated metal interconnects appear as dark features (e.g., green arrow in *A*) and SU-8–only elements appear as lighter gray features (e.g., red arrow in *A*) at the middle of each image. The DIC images were acquired from the same region of the same tissue slices used to obtain the confocal microscopy images in Fig. 2 *A*–*C*; the mesh features imaged by DIC are shown as pseudocolored blue in the composite images shown in Fig. 2 *A*–*C*. (Scale bars in all images, 100 μm.)

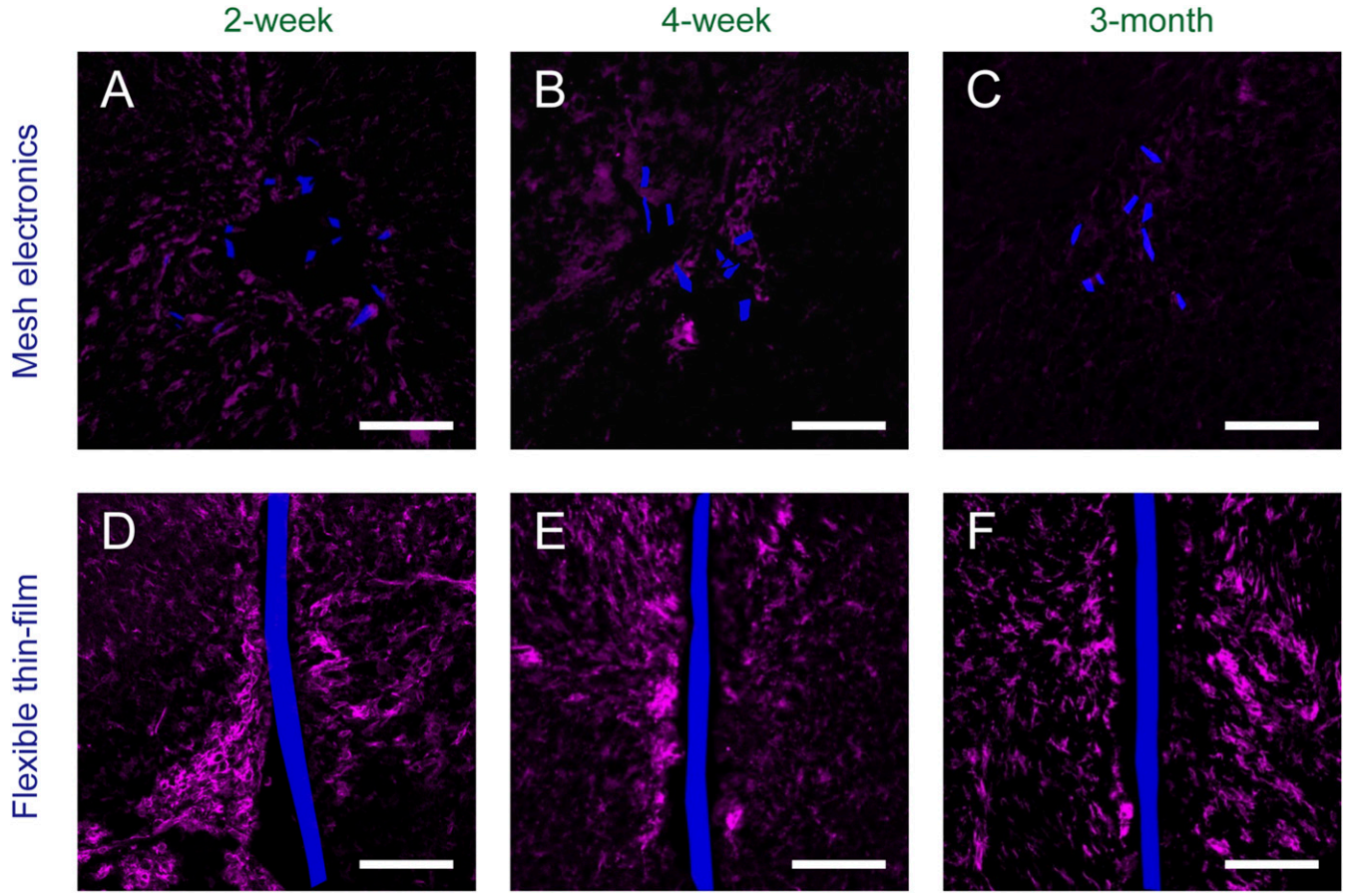

Fig. S2. Time-dependent histology of chronically implanted mesh electronics (*A*–*C*) and flexible thin-film probes (*D*–*F*) in mice brains (horizontal sections). Tissue slices are labeled with Iba-1 (magenta) to highlight microglia; mesh electronics and flexible thin-film probes were imaged by DIC and are pseudocolored blue. (Scale bars in all images, 100 μm.)

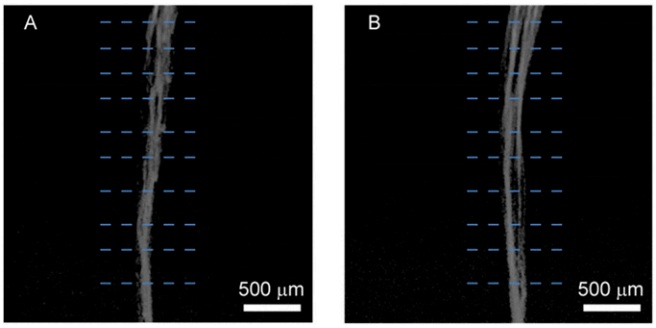

Fig. S3. (*A* and *B*) Micro-CT images of two different mesh electronics implanted into a mouse brain in an acute manner. Diameter measurements of each mesh at 10 randomly selected positions (blue dashed lines) resulted in average diameters of 163 ± 40 μm for the mesh in *A* and 215 ± 44 μm for the mesh in *B*.

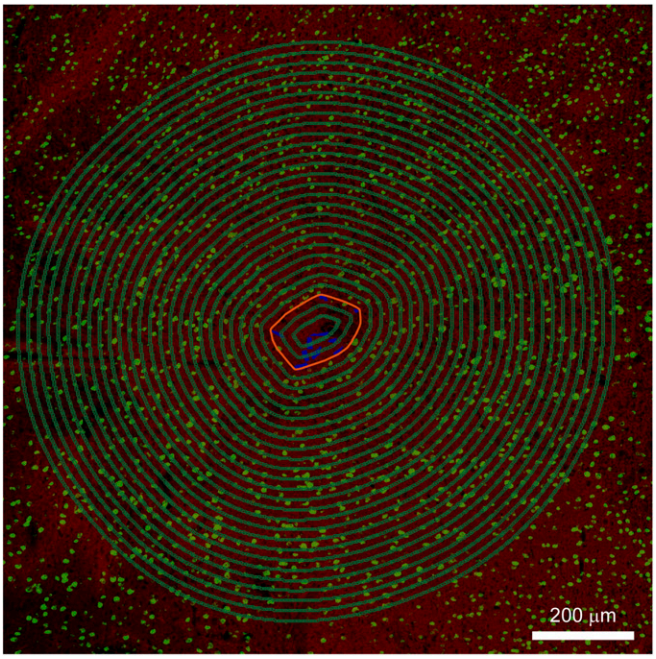

Fig. S4. Schematic of the fluorescence intensity data analysis based on the zoomed-out image (3×3 composite image recorded directly in the Tile Scan mode, where each component image of the Tile Scan had a field of view of 425 μm × 425 μm) of Fig. 2*B*, *IV* with a field of view of 1,275 μm × 1,275 μm. The red-orange polygon indicates the mesh boundary that is drawn according to the method described in SI Text. The green polygons in the image indicate groups of pixels that share the same distance from mesh boundary. The space between two adjacent green polygons is 20 μm.

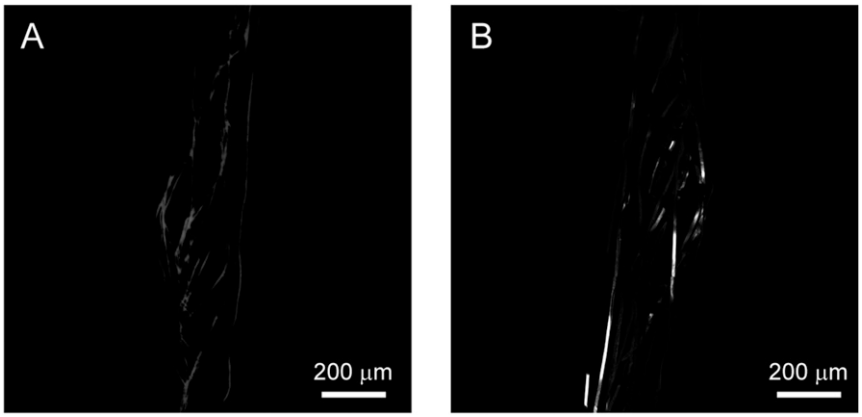

Fig. S5. Mesh electronics images from the sagittal tissue slice. Images were acquired in reflection mode of the confocal microscope (see *SI Text* for details). (*A* and *B*) Reflection images of mesh electronics from side-A and side-B, respectively, of the sagittal tissue slice images shown in Fig. 4 *A* and *B*. Each of the images are 3×3 composite images recorded directly in the Tile Scan mode, where each component image of the Tile Scan had a field of view of 425 μm × 425 μm. The mesh electronics elements were extracted from these reflection images and then merged with corresponding confocal fluorescence images shown in Fig. 4 (*SI Text*).